TWELFTH EUROPEAN ROTORCRAFT FORUM

Paper No. 79

EXPERIMENTAL APPLICATION OF STRAIN PATTERN ANALYSIS (SPA) - WIND TUNNEL AND FLIGHT TEST RESULTS

A. R. Walker

D. B. Payen

Royal Aircraft Establishment
FARNBOROUGH, England

22-25 September 1986

Garmisch-Partenkirchen
Federal Republic of Germany

Deutsche Gesellschaft für Luft- und Raumfahrt e.V. (DGLR)
Godesberger Allee 70, D-5300 Bonn 2. FRG

Copyright
©
Controller HMSO
London 1986

LIST OF CONTENTS

EXPERIMENTAL APPLICATION OF STRAIN PATTERN ANALYSIS (SPA) - WIND TUNNEL AND FLIGHT TEST RESULTS

by

A. R. Walker

D. B. Payen

Royal Aircraft Establishment, Farnborough, England

ABSTRACT

Further experimental application of Strain Pattern Analysis (SPA) to derive rotor blade deformations is described. The SPA technique has now been extended to derive not only the vibration mode shapes of a rotating blade, but also the instantaneous deformation shape at consecutive azimuth stations around the rotor disc. This technique has been successfully applied to both a dynamically scaled rotor model tested in the RAE 24ft Wind Tunnel, and a Puma helicopter used in flight research at RAE Bedford. Instantaneous blade deformations around the rotor disc are presented for both the model and helicopter rotor blades. These results are compared with corresponding calculated deflections.

1 INTRODUCTION

With the advent of new and more complex helicopter rotor blade designs, larger couplings between the flap, lag and torsion components of motion are being considered. Such couplings influence almost every aspect of rotor dynamic behaviour, and analytical investigations of their effects rely heavily on an accurate mathematical model for predicting the modes of vibration of the blade. Many calculation methods giving mode shapes and frequencies are available, but experimental verification is lacking. The technique of Strain Pattern Analysis (SPA) has been developed at RAE, therefore, to derive the mode shapes of a rotating blade from its measured strains. This technique has now been extended to derive not only the mode shapes, but also the instantaneous deformation shape of the blade at any azimuth station around the rotor disc in forward flight.

The technique has been applied successfully to a simple rotor model, as reported previously[1,2]. Recently, however, SPA has been applied to two more complex and different rotor systems[3,4]. The first is the three-bladed rotor model fitted with a dual load path hub currently used for experimental research in the RAE 24ft Wind Tunnel, some initial results of which were reported at the 1984 Forum[5]. The second application of SPA is to a full-scale articulated rotor system, that of the Puma helicopter used for flight research at RAE Bedford[6]. Instantaneous blade deformations around the azimuth are presented for both the model and full-scale helicopter rotor blades. Preliminary comparisons with corresponding deflections calculated by computer programs developed by Westland Helicopters Ltd[7] and by RAE[8] are also presented.

2 THEORETICAL BACKGROUND

The method used to derive the mode shapes of a rotating blade by the technique of Strain Pattern Analysis (SPA) has been presented at previous Forums[1,2], thus only a brief résumé of the theory will be given here.

The SPA technique is simple to apply in principle. It consists of first recording the strain patterns along the blade, together with their corresponding displacements, for a number of vibration modes of the non-rotating blade. These are known as the calibration strain and displacement patterns respectively. The measured strain response of an unknown mode of the rotating blade is first represented as a linear sum of the calibration strain patterns by using a least-squares error fitting procedure. The mode shape (or instantaneous deformation) of the rotating blade is then assumed to be given by the same linear sum of the calibration displacement patterns.

For the application of the technique to be valid, two conditions must be satisfied

(a) the relationship between any set of strain patterns and the corresponding displacement patterns (mode shapes) must be unique;

(b) sufficient non-rotating modes must be defined, such that a linear combination of them will provide a good approximation to the rotating mode.

If S is the matrix of the strain responses of the modes of the non-rotating blade and D the matrix of corresponding displacements, ie the calibration modes, then Gaukroger et al[1] have shown that, by using a least-squares fitting procedure, the vector $\underline{a}$ representing the proportions of each calibration mode in some unknown mode is given by

$$\underline{a} = (S^T S)^{-1} S^T \underline{x} \tag{1}$$

where $\underline{x}$ is the vector of strain responses of the unknown mode shape for some test condition. It follows that

$$\underline{d} = D\underline{a} = D(S^T S)^{-1} S^T \underline{x} \tag{2}$$

where $\underline{d}$ is the vector of displacements of the unknown mode shape associated with the strain responses $\underline{x}$.

To make a qualitative assessment of the match between the strain patterns measured during the experiments and those derived by SPA from the calibration modes, a strain-fit check (SFC) based on standard deviation is calculated from the expression

$$SFC = \left[\frac{1}{n}\sum_{i=1}^{n}(y_i - \bar{y})^2\right]^{\frac{1}{2}} \tag{3}$$

where y_i = strain error term = $\left| \sum_{j=1}^{n} S_{ij} a_j - x_i \right|$

$\bar{y}$ = mean of the strain errors = $\frac{1}{n} \sum_{i=1}^{n} y_i$

i = the ith vector component
j = the jth calibration mode
n = total number of strains in set

Obviously, as the value of SFC tends to zero, one can have more confidence that the corresponding derived blade shape is correct.

3 WIND-TUNNEL MODEL EXPERIMENT

3.1 Dual load path rotor model

It is not intended to describe extensively the rotor model used for the SPA experiment in the RAE 24ft Wind Tunnel, as full details have already been given at the 1984 Forum[5]. Briefly, the model has a dual load path (DLP) hub (sometimes referred to as split load path) which separates the hub structural elements carrying the centrifugal loads from those providing flap and lag flexibility. The centrifugal loads are transmitted from the blade through a sweep/pre-cone link and eventually to earth, ie the hub, by an elastomeric bearing which behaves as a universal ball joint and allows rotation about any axis. Flap stiffness is provided by two flexures, lag stiffness by an elastomer situated between a spherical bearing (to allow blade pitch via the pitch arm) and the flap flexures. An idealised diagram of the DLP rotor model, together with its main characteristics, is shown in Fig 1.

The model has 3 rotor blades of GFRP construction with a RAE 9642 aerofoil section. The rotor diameter is 3.6 m, the blade chord 0.14 m and the nominal operating rotational speed is 600 rpm. Although not a scale model of any particular current system, the model is dynamically representative of typical modern rotors except that its torsional stiffness is high due to the method of rotor blade manufacture (see Ref 5). Fig 2 shows the calculated vibration mode frequencies with varying rotor speed. The first torsional mode is at about 11Ω at the nominal rotor operating speed. Further details of the rotor model are given in Ref 5.

3.2 SPA instrumentation

Previous experience with SPA[2] has shown that positioning of the strain gauges on the rotor model is crucial to the accuracy of mode shape derivation of a rotating blade. A computer study of the application of SPA to the DLP rotor model was completed[9], therefore, before instrumentation of the model commenced. The results of this study confirmed earlier conclusions that comprehensive strain gauging of the root components was necessary to ensure accurate results.

Consequently, the rotor model was instrumented with a total of 55 4-arm strain gauge bridges to measure flap, lag and torsional components of motion (22 flap, 17 lag, 16 torsion). In addition, the root lead/lag and pitch motions were measured with linear and rotational potentiometers respectively. These two latter measurements were treated as pseudo-strains in the subsequent strain

pattern analysis of wind tunnel data[1]. The strain gauge positions are shown in Fig 3a. Unfortunately, due to lack of channels in the rotor hub electronics, some of these positions could not be used, and therefore a reduced set of strain gauges (47) were selected for the tests. Subsequently, some of these gauges malfunctioned during both the calibration and wind-tunnel tests, and these also had to be neglected in the analysis. The remaining strain gauge positions (42 in total) are shown in Fig 3b. Non-rotating calibration modal displacements were measured for the three components of motion with miniature Entran accelerometers (type EGA-125F-100). Flap and lag motions were measured at 13 radial stations at the blade ¼-chord. Torsional motions were obtained at 10 radial stations from differential readings of accelerometers placed at the rotor blade trailing edge and those measuring flap at the ¼-chord. These positions are shown in Fig 3c. When the torsion component of a mode is plotted, it is expressed in terms of displacement, ie as the product of the torsion angle and the blade chord, and this enables the composite mode shape to be 'normalised' with respect to the largest component of motion. A similar procedure also applies to the results obtained for the Puma helicopter.

3.3 Non-rotating calibration modes

As stated previously, the calibration modes of the system are the strain and corresponding displacement patterns of the modes of the non-rotating blade. Mode excitation was obtained either by a number of electromagnetic vibrators located along the rotor blade, or by just one placed at the rotor hub. The excitation was controlled by RAE MAMA equipment[2] which automatically maintained a resonance condition by ensuring a quadrature phase relationship between the force input and the response of a continuously monitored strain gauge sensitive to motion in the main component of the mode under investigation. Calibration modes were measured with a Hewlett Packard 5451C Fourier Analyser computer through an Analogic Data Acquisition System (DAS). The strain gauges had a power supply of 5V and the outputs were amplified by a factor of 300 by Vishay signal conditioning equipment. The accelerometers also had a 5V power supply, but their outputs were amplified by a factor of 500.

Strain and corresponding displacement patterns were measured for four types of calibration mode, ie with the rotor blade pitch-fixed and pitch-free for both normal mode and hub excitation. More details of these can be found in Ref 3. A selection of the modes was used to form the calibration matrices S and D (see section 2) for subsequent strain pattern analysis of wind-tunnel data, and these are shown in Fig 5. The description of each mode arises from the largest component of motion within the mode. Only the major components of each mode are shown, although all components are used in application of the SPA technique.

3.4 Wind-tunnel tests

The SPA experiment on the 3-bladed DLP rotor model was conducted in the RAE 24ft Wind Tunnel. A description of the tunnel can be found in Ref 5. The rotor model is mounted on a tower 4.5 metres tall, thereby locating the rotor in the centre of the tunnel flow. The tower is supported by the under-floor balance used to measure lift and drag. The upper part of the tower may be tilted to simulate forward flight trim, and all SPA tests were conducted with a 5° forward tilt. The rotor model in the tunnel is shown in Fig 4.

Strain gauge signals, both for SPA purposes and for safety monitoring of all three blades and pitch links, were amplified on a 45-channel system (100x)

mounted above the rotor hub. Thence, via sliprings and a second set of amplifiers (3x), the signals were passed to a 64-channel DAS on a Hewlett Packard 1000e series computer which was used to process and record the data. Various gains and offsets were applied as necessary to each channel, after which the signals passed through filters to 'sample-and-hold' electronic circuits. These enabled all 64 channels to be sampled simultaneously, ie at one azimuth position on the rotor disc. More details of this system can be found in Ref 5. The strain gauge data were then multiplexed, digitised and written to external memory before transfer to a VAX 11/780 computer for analysis.

A large amount of strain data was recorded during the SPA tunnel tests to cover a range of different thrust, rotor speed and advance ratio conditions. These are shown in Table 1. Strain data were recorded at 256 stations/rev (to give a blade strain pattern at approximately every 1.4° of azimuth) and averaged over 16 revolutions of the rotor. Unfortunately, with the limited number of channels available on the rotor hub, it was impossible to record all the SPA strain gauge signals at once. The tests, therefore, were conducted in two stages, designated A and B . Approximately two-thirds of the selected SPA strain gauge signals were recorded in the A run, the remainder in the B run. Some common channels (in all three components of motion) were recorded for comparison purposes in both cases. The two sets of strain patterns were matched together during subsequent analysis on the VAX computer using the DATAMAP program at RAE[10].

Whilst the model was in the wind tunnel, it was continuously monitored by a TV camera for safety reasons. By strobing the rotating model at the correct frequency it was possible to estimate on the TV video screen, for the SPA instrumented blade only, the tip motion in flap, lag and pitch at the 240° azimuth station. The blade chord was used as a reference length.

4 PUMA HELICOPTER EXPERIMENT

4.1 Main rotor system and SPA instrumentation

The aircraft used in the SPA experiment was the flight research Puma helicopter from RAE Bedford[6]. This was the first time SPA had been applied to a full-scale rotor system. It is unnecessary to describe in detail the main rotor system of the Puma. Briefly, it consists of a 4-bladed rotor, with a hub fully articulated in flap, lag and pitch, and an integral rotor brake. The rotor has a diameter of 15 m and a chord of 0.533 m. The nominal rotor operating speed is 265 rpm, although some of the SPA flight tests were conducted at a lower speed of 240 rpm. Further details of the rotor can be found in many standard texts.

Basically, the same rules governing the SPA instrumentation of the DLP rotor model were applied to the Puma main rotor, although in the latter case many more strain gauges were used. A total of 96 4-arm strain gauge bridges measuring flap, lag and torsion components of motion (32 gauges for each component) were attached to the main rotor at approximately equi-spaced stations. In addition, the flap, lag and torsion root motions were measured with linear and rotational potentiometers (these measurements are standard on the Bedford Puma). Further details of the instrumentation techniques are provided in Ref 6. The strain gauge positions are shown in Fig 6a. Again, as with the DLP rotor model, a few strain gauges malfunctioned during calibration and flight tests, and these were neglected in the subsequent analysis of the flight data. The remaining 86 strain gauges (29 flap, 26 lag, 31 torsion) are shown in Fig 6b. The calibration mode shapes were measured with miniature accelerometers (the same type as

used for the model rotor). Flap and lag motions were measured at 14 radial stations at the blade ¼-chord; torsional motions were obtained at 11 radial stations from differential flap and trailing edge measurements. The accelerometer positions are shown in Fig 6c.

4.2 Ground calibration tests

The calibration modes were recorded at RAE Farnborough in November 1984. The tip of the SPA instrumented rotor blade was suspended from the hangar roof by a long, elastically soft cord, in order to lift the blade off the root flap stops. Mode excitation was obtained by a number of electromagnetic exciters located along the rotor blade. There were two at the blade root operating in-phase for flap, the same two operating in anti-phase for torsion, and one at the blade tip for lag. Excitation was controlled by RAE MAMA equipment, as detailed in section 3.2. The calibration displacement patterns (mode shapes) were measured with the Hewlett Packard DAS described in section 3.3. The calibration strain patterns were measured on the Puma helicopter DAS described in Ref 6. The two systems were synchronised to record the displacement and strain patterns simultaneously without phase differences. The Puma helicopter during the ground calibration tests is shown in Fig 7, together with the Hewlett Packard computer system.

A total of 14 calibration modes were recorded (7 flap, 4 lag, 3 torsion) during the ground tests. The blade pitch link was connected to the swash plate and the helicopter hydraulic system was activated. The calibration modes are shown in Fig 8. As with the DLP rotor model, only the major components of each mode are shown for clarity, although all components are used in the flight data analysis.

4.3 Flight tests

The SPA flight tests on the Puma helicopter main rotor were conducted at RAE Bedford. A large amount of strain data was recorded over a range of thrust coefficient/solidity values and advance ratio conditions for two rotor speeds (265 and 240 rpm). These conditions are shown in Table 2. Strain data were recorded at 256 stations/rev on the 64-channel DAS used in flight research. As in the wind-tunnel tests, the strain pattern data had to be measured in two sets because of the lack of data recording channels. The first measured over half the strain data simultaneously using 'sample-and-hold' circuits. These were amplified, passed through the sliprings and recorded as described in Ref 6. Switching circuits in the hub electronics selected the remaining strain gauges, and these were also recorded simultaneously. Both sets of strain gauge responses were recorded before the rotor blade had moved to the next azimuth station. Obviously, some phase differences did occur between the two sets of data but these were considered to be negligible. Channels common to both were recorded for comparison when the two data sets were matched together.

5 DISCUSSION OF RESULTS

5.1 Calculation methods

Computer models of the DLP and the Puma rotor systems were created from their respective mass, stiffness and inertia distributions. For the former, the flap and lag load paths were modelled as two springs to earth with finite values of stiffness[5,9]. Vibration modes for the rotor systems were calculated by a computer program developed by Westland Helicopters Ltd based on the work of King[7]. Subsequently, blade loads and deflections were calculated from these

modes by the RAE Rotor Loads program developed by Young[8]. This latter program uses a vortex ring wake model and includes an interactive near wake and a model of the dynamic stall process.

Both the theoretical predictions and the SPA derived displacements require a sign convention for the blade motion. The convention is positive for flap motion upwards, lag motion backwards and pitch motion nose up. Note also that in the following discussion, 'calculated' results refer to those produced by the theoretical prediction methods, 'measured' results are those recorded during either the wind tunnel or flight experiments, and 'derived' results refer to those produced by the SPA technique.

5.2 Wind-tunnel tests

Examples of the match around the rotor disc between strain gauge responses for the SPA A and B runs are presented in Figs 9 and 10 for two test conditions, ie advance ratios $\mu = 0.2$ and $\mu = 0.34$ respectively. Both tests were conducted at a rotor speed of 600 rpm and a thrust of 900 N. Although the match between the A and B strain responses is not perfect, the variation of strain around the rotor disc is the same, apart from some difference in magnitude which itself varies with strain gauge position. This correlation of the azimuthal variation gives confidence that the strain responses for the two runs can be combined, and initially the strain patterns have been analysed without any adjustment to the difference in magnitude. The effect of the B set of strains by a factor in order to match the A set more closely is still under consideration.

Examples at one azimuth station (ie 240°) of blade shape derivation using the SPA technique are presented in Figs 11 and 12 for the same two test conditions described above. Fig 11a shows the match between the strain patterns measured during the wind-tunnel test and those constructed from the linear combination of the calibration strain patterns (see Fig 5) for the lower advance ratio condition of $\mu = 0.2$. As can be seen clearly, the match between the strains is good, giving confidence that the calibration modes set is sufficiently complete. The proportions of the calibration modes used in the SPA derivation are shown in Fig 11b, together with an estimation of their statistical variance[11]. The usefulness and accuracy of variance with SPA is still under investigation. The resulting SPA derived blade shape is shown in Fig 11c, together with some preliminary calculated displacements and also the blade tip motions as measured on the TV monitoring screen. The match between the calculated and SPA derived lag motions is good, although there are some discrepancies for the flap and pitch motions. The SPA derived flapping motion is somewhat greater than that predicted by theory. The reasons for this will be discussed later. It is interesting to note that the measured tip motions do not match up very well with either the calculated or SPA derived results.

Table 3 shows the percentage contribution of each calibration mode to the SPA derived tip displacement/rotation for the same test condition. This shows clearly that, for the flap and lag motion, the SPA derived blade shape is comprised mainly of the fundamental bending mode, with 1st and 2nd harmonics making up the balance. Higher order modes make a negligible contribution to the overall blade shape. For blade pitch, the rigid body pitch calibration mode contributes most to the overall motion, but this is not surprising considering the high torsional stiffness of the rotor blade. However, many other modes (eg the first elastic torsion mode; lower order flap and lag modes) subtract from the overall blade pitch motion. The contributions from the flap and lag modes may account for the discrepancies in the calculated and SPA derived pitch

motions, because they introduce into the calibration modes other sources of torsional motion which may invalidate the first assumption made in section 2. This problem is still being investigated.

The results for the higher advance ratio condition of $\mu = 0.34$ are presented in Fig 12. Again, the match between the strain patterns is good (Fig 12a), using similar mode proportions (Fig 12b). The comparison between the calculated and SPA derived blade shapes (Fig 12c) is good for lag, with some discrepancies for flap and pitch. Percentage contributions from each calibration mode to the SPA derived tip displacements/rotations are also shown in Table 3. This confirms the earlier observation that the blade shape consists mainly of a combination of the lower order modes. It should be noted, that the azimuth station of 240° presented in Figs 11 and 12, exhibits the worst correlation between blade pitch as calculated by the theoretical prediction methods and that derived by SPA. Better correlation is seen at other stations around the rotor disc as shown in Figs 13 and 14.

The variation of strain and displacement of the blade around the whole of rotor disc for the same two test conditions ($\mu = 0.2$ and $\mu = 0.34$) is shown in Figs 13 and 14 respectively. Each illustrates the variation in strain, as measured during the wind-tunnel tests, and blade shape, as calculated and as derived by SPA. In both cases for most azimuth stations, the comparison between calculated and SPA derived lag and pitch motions is good, but there are discrepancies for the flapping motion. In the latter case, the best match is in the azimuth range 240-300°, ie the retreating side of the rotor disc. Note that the maximum displacement for the higher advance ratio condition (Fig 14) is 98.24 mm, approximately 30% greater than for the lower advance ratio case (Fig 13).

Let us consider some possible explanations for the discrepancies between calculated and SPA derived results. First, consider the theoretical prediction methods. Although the input data to the computer programs were the best available, there is concern that the stiffness and inertia distributions of the rotor are in error. Further work is in progress at RAE to determine these distributions more accurately[12]. Also, the programs themselves over-simplify the representation of the elements of the dual load path hub. For the wind-tunnel experiment there are two possible sources of error. As stated previously, earlier applications of SPA have shown that root strains, especially in the fundamental flap modes, greatly affect the subsequent derived blade motion[2]. Usually poor definition of the root flap strains leads to an over-emphasis of the fundamental flap mode in the SPA derived blade shape, and in an attempt to overcome this difficulty, the root flap flexures were comprehensively instrumented with flap strain gauges (see Fig 3a). It has also been stated (see sections 3.2 and 3.4) that some of the gauges could not be selected for the experiment due to the lack of channels in the rotor hub electronics, even with recording the wind tunnel strain patterns in two sets. Unfortunately, some of these strain gauges were on the flap flexures (see Fig 3b). Therefore, the root flap strains of the blade may not have been as well defined as was necessary for SPA, leading to an over-emphasis of the contribution from the fundamental flap calibration mode. Finally, but less importantly, there is some error introduced into the SPA derivation by the differences between the SPA A and B runs.

5.3 Flight tests

Similar results have been obtained for the SPA experiment with the Puma helicopter rotor system. However, in this application of SPA, because the rotor system is articulated, the total blade displacement shape is assumed to consist of two parts. The first is the elastic bending (or twisting) of the rotor blade

which is derived by SPA from the measured strain gauge responses. The second is the rigid body motion of the blade about the root hinges for the three components of motion. These rigid body motions are derived from the differences between the root angles measured during the flight tests and the root angles corresponding to the SPA derived blade elastic motion.

Figs 15 to 20 show comparisons between calculated and SPA derived blade shapes for one flight test condition, ie at a forward speed of 80 knots, a thrust coefficient/solidity value T_c of 0.09 and an advance ratio μ of 0.193 . Figs 15 and 16 present results for the advancing side of the rotor disc. The former shows strain patterns and blade shapes for the elastic motion of the rotor at an azimuth angle of 90°. The match between the measured strain patterns and those constructed from the linear combination of the calibration modes is shown in Fig 15a, the dominant strain response being that in lag. The resultant elastic blade shape is shown in Fig 15c. The comparison between calculated and SPA derived flap motions is good, but not so for the pitch and lag motions. For the latter, the two blade shapes are completely out of phase. The total blade motion for the same azimuth angle is shown in Fig 16. The comparison between calculated and derived motions is good for the lag motion, but less so for flap and pitch. Similar results are shown in Figs 17 and 18 for the retreating side of the rotor disc at 270° azimuth. Note that here, as expected, the total blade shape (Fig 18) contains more flap and pitch motion than on the advancing side. Table 4 shows the percentage contributions of the calibration modes to the SPA derived elastic motion of the blade for both azimuth angles. As for the wind-tunnel model, most of the blade flap and lag motion is made up from combinations of the lower modal harmonics. The torsional elastic response, however, is comprised not only of torsional calibration modes, but also of torsional responses from flap and lag calibration modes which may account for the discrepancies between the calculated and SPA derived elastic motions as explained previously for the wind tunnel model.

The variation of the blade motion around the rotor disc is presented in Figs 19 and 20 for the elastic and total blade motions respectively. For the elastic motion (see Fig 19), the match between calculated and SPA derived flap is good apart from the azimuth range 150-240°, ie the front sector of the rotor disc. The correlation for pitch and lag motions is not so good. For the total blade motion (see Fig 20), the match is good for all three components of motion around the whole of the rotor disc, apart from some discrepancy for flap in the azimuth range 0-90°. Note that the elastic blade motion comprises only 35% of the total blade shape, the rest being rigid body response.

Let us consider a possible explanation for the discrepancies in the lag motion between the calculated and SPA derived results. Young has already found in earlier flight experiments with the Puma helicopter[13], that the measured and calculated strains and bending moments are out of phase with one another. Also, there is a completely different modal content shown between experiment and theory, with the latter producing poorly predicted results for edgewise (lag) bending moments. This, in turn, introduces errors in the predicted lagwise deflections. It is thought that the errors in the calculations may arise from exclusion from the theoretical model of the root lag damper, the characteristics of which are not sufficiently well understood.

6 CONCLUDING REMARKS

Two experiments have been conducted at RAE to extend the technique of Strain Pattern Analysis (SPA). Now, not only mode shapes of a rotating blade

can be derived experimentally for comparison with theoretical prediction methods, but also the instantaneous motion of a helicopter blade as it moves around the rotor disc. The first experiment used a model rotor tested in the RAE 24ft Wind Tunnel; the second applied SPA to a Puma helicopter rotor system. Some preliminary comparisons between calculated blade deflections and those derived by SPA have been made. The discrepancies between the two have highlighted some of the problems that can occur when applying the SPA technique to rotor systems.

In the case of the wind-tunnel experiment, the flapping motion of the blade has been over-emphasised by SPA. This occurred because an insufficient number of strain gauges was selected to define the strain responses of the flap flexures at the root of the rotor model. Also, recording the wind-tunnel strain patterns in two sets will have introduced some experimental error into the analysis. Both these problems occurred due to the lack of data recording channels. For future tests, the wind-tunnel model will have an increased number of slip-rings and corresponding data recording channels (80 in total), and a further SPA experiment may take place to eliminate the sources of these errors. Additionally, an investigation of the proportions and types of calibration modes (coupled or uncoupled) used by SPA to derive blade shapes will be undertaken.

It is also known that the theoretical prediction methods are not fully representative. For the wind-tunnel model, there is concern that the theoretical modelling of the dual load path rotor system by springs-to-earth is oversimplified. In the case of the Puma helicopter rotor system, the exact characteristics of the lag damper are unknown and therefore it is impossible to be fully confident that it is represented correctly in the prediction methods. Also, for both the wind tunnel and flight test results, a comparative study of calculated blade loads with those obtained from the measured strain gauge responses will be made to assess the accuracy of the theoretical prediction methods.

Acknowledgment

The authors would like to thank members of the wind-tunnel section of Helicopters Division at RAE Farnborough, and the flight research team at RAE Bedford (especially Mr F.B. Moulang and Mr C. Handley), without whose invaluable assistance the experiments could not have taken place.

Table 1

WIND TUNNEL TEST PARAMETERS AND CONDITIONS FOR THE SPA EXPERIMENT ON THE DLP ROTOR MODEL

Thrust (N)	Rotor speed (rpm)	Pre-cone (degs)	Sweep (degs)	Advance ratio
600	600	5	5	0 to 0.34
900	600	5	5	0 to 0.34
1050	600	5	5	0 to 0.34
417	500	5	5	0 to 0.34
267	400	5	5	0 to 0.34
150	300	5	5	0 to 0.34

Table 2

FLIGHT TEST PARAMETERS AND CONDITIONS FOR THE SPA EXPERIMENT ON THE PUMA HELICOPTER MAIN ROTOR

Flight case	Thrust coefficient / solidity	Rotor speed (rpm)	Forward speed (knots)	Advance ratio
F600	0.073	265	40 to 158	0.10 to 0.39
F594	0.078	265	0 to 160	0.00 to 0.40
F599	0.088	265	75 to 124	0.18 to 0.36
F598	0.075	240	67 to 100	0.18 to 0.27
F601	0.075	240	90 to 151	0.24 to 0.41
F596	0.080	240	80 to 145	0.22 to 0.40
F597	0.090	240	76 to 142	0.21 to 0.39
F602	0.07 to 0.09	265	Hover	
F603	0.08 to 0.102	240	Hover	
F604	0.08 to 0.09	240	Hover	

Table 3

PROPORTIONS OF CALIBRATION MODES CONTAINED IN TIP DEFLECTION FOR THE WIND-TUNNEL MODEL

AZIMUTH ANGLE = 240°

Calibration mode		Advance ratio = 0.2			Advance ratio = 0.34		
No.	Description	Flap	Lag	Pitch	Flap	Lag	Pitch
1	rigid pitch	-	-	150%	-	-	132%
2	1st flap	95%	3%	-15%	92%	4%	-9%
3	1st lag	-	-110%	-10%	-	-112%	-5%
4	2nd flap	9%	-	-	9%	-	-
5	3rd flap	-5%	-	-2%	-3%	-	-7%
6	1st torsion	-	-	-15%	-	-	-5%
7	2nd lag	-	-13%	-4%	-	-13%	-2%
8	4th flap	-	-	-3%	-	-	-4%
9	5th flap	-	-	-	-	-	-
10	3rd lag	-	23%	-	-	19%	-
11	2nd torsion	-	-	-	-	-	-
Total motion		59 mm	-29 mm	3.6°	79 mm	-31 mm	8.1°

Table 4

PROPORTIONS OF CALIBRATION MODES CONTAINED IN TIP DEFLECTION FOR THE PUMA HELICOPTER ROTOR SYSTEM

Calibration mode		Azimuth = 90°			Azimuth = 270°		
No.	Description	Flap	Lag	Pitch	Flap	Lag	Pitch
1	1st flap	96%	-14%	40%	86%	-21%	45%
2	1st lag	-9%	-80%	40%	-5%	-69%	25%
3	2nd flap	15%	-	-	20%	-	-
4	3rd flap	-3%	-	-	-	-	-
5	2nd lag	-	-4%	15%	-	-8%	23%
6	1st torsion	-	-	12%	-	-	15%
7	4th flap	-	-	-	-	-	-
8	5th flap	-	-	-	-	-	-
9	3rd lag	-	-	-	-	-	4%
10	2nd torsion	-	-	-	-	-	-8%
11	6th flap	-	-	-8%	-	-	-
12	4th lag	-	-	-	-	-	-4%
13	7th flap	-	-	-	-	-	-
14	3rd torsion	-	-	-	-	-	-
	Total motion	236 mm	-132 mm	-2.8°	346 mm	-115 mm	-3.3°

REFERENCES

No.	Author	Title, etc
1	D.R. Gaukroger D.B. Payen A.R. Walker	Application of strain gauge pattern analysis. Paper No. 19, 6th European Rotorcraft Forum (1980)
2	A.R. Walker	Further application and development of strain pattern analysis. Paper No. 7.2, 8th European Rotorcraft Forum (1982)
3	A.R. Walker	Experimental application of strain pattern analysis to a dynamically scaled rotor model. RAE Technical Report (to be published)
4	A.R. Walker D.B. Payen	Application of strain pattern analysis to Puma helicopter XW 241. RAE Technical Report (to be published)
5	J.T. Cansdale R.J. Marshall P.A. Thompson	Tests on a new dynamically scaled model rotor in the RAE 24ft Wind Tunnel. Paper No 98, 10th European Rotorcraft Forum (1984)
6	F.B. Moulang	A review of RAE experimental techniques for rotor dynamics and aerodynamics. Paper No 96, 10th European Rotorcraft Forum (1984)
7	S.P. King	Blade equations by Hamiltons Method using an ordering scheme. WHL Report No. GEN/DYN/209N (1980)
8	C. Young	Prediction of aerodynamic loads on rotorcraft. Paper No. 11, AGARD-CP-334 (1982)
9	A.R. Walker	A computer study of the application of strain pattern analysis to a model split load path rotor system. RAE Technical Memorandum Mat/Str 1041 (1984)
10	C. Young	DATAMAP and its implementation at RAE. RAE Technical Memorandum Mat/Str 1011 (1983)

REFERENCES (concluded)

No.	Author	Title, etc
11	J.C. Copley	Numerical analysis of vector responses. RAE Technical Report 80135 (1980)
12	C. Hatch A.R. Lee	Determination of the structural properties of helicopter rotor blades by theoretical and experimental methods. Paper No. 67, 12th European Rotorcraft Forum (1986)
13	C. Young	A comparison of the measured and predicted stresses on the rotor blades of three helicopters. RAE Technical Report 85027 (1985)

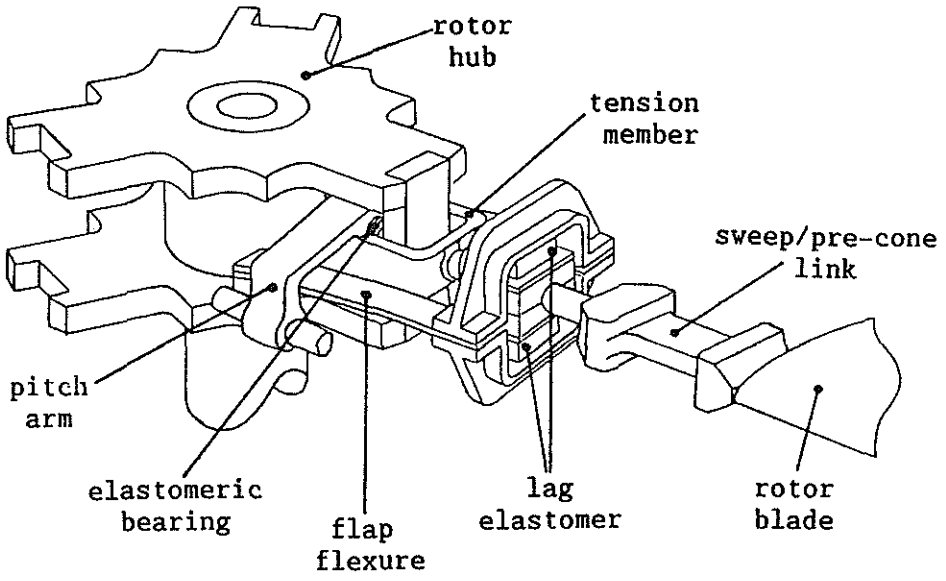

ROTOR MODEL CHARACTERISTICS

number of rotor blades	=	3
aerofoil section	=	RAE 9642
rotor radius	=	1.80 m
rotor blade chord	=	0.14 m
rotor blade pre-cone	=	5^{o} (at 5% rotor radius)
rotor blade sweep	=	5^{o} (at 19% rotor radius)
rotor blade twist	=	4.4^{o}/m
effective hinge offset	=	14% of rotor radius
blade flap stiffness	=	167 Nm^2
blade lag stiffness	=	5900 Nm^2
blade torsional stiffness	=	159 Nm^2

Fig 1 Dual load path (DLP) rotor model

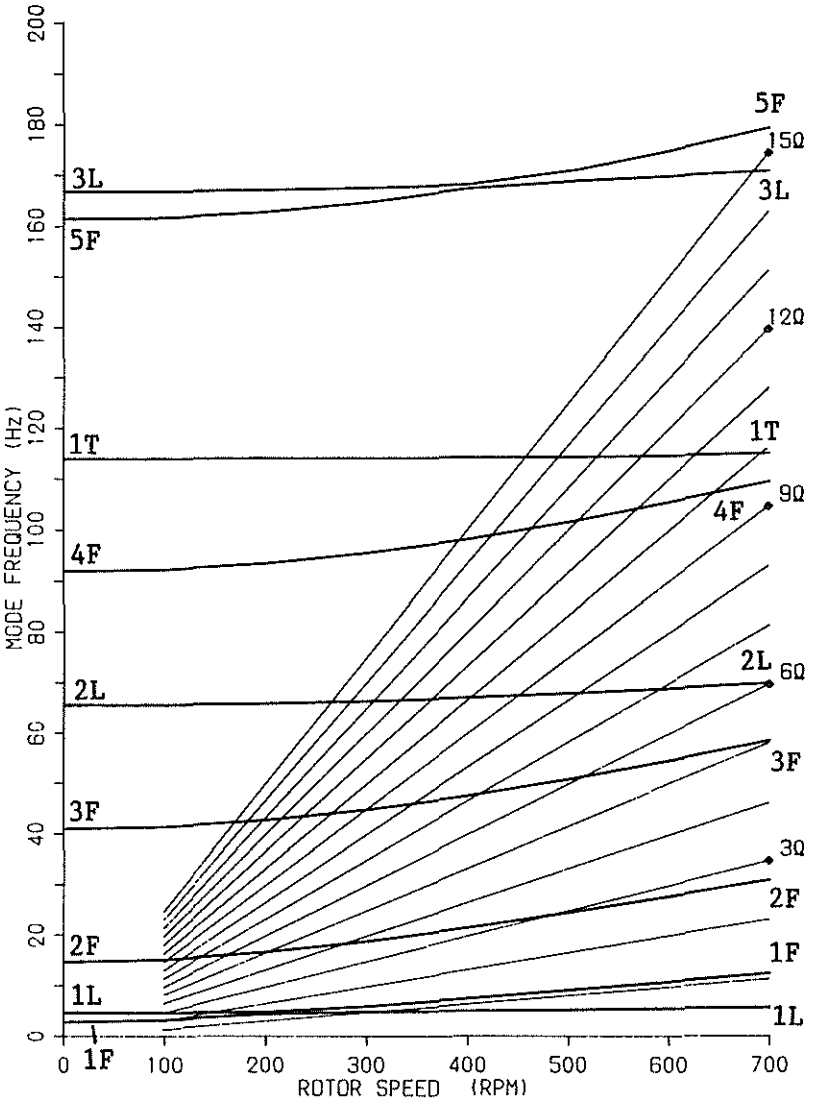

F = flap mode
L = lag mode
T = torsion mode

Fig 2 Mode frequencies vs rotor speed for the DLP rotor model

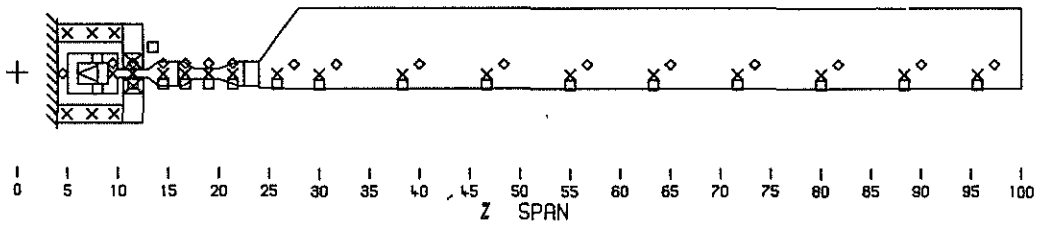

(a) strain gauge positions

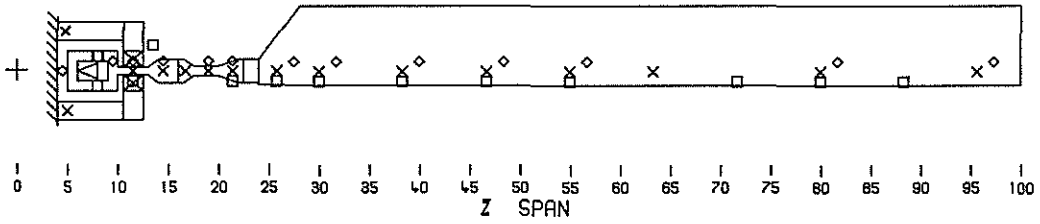

(b) strain gauge positions used in SPA

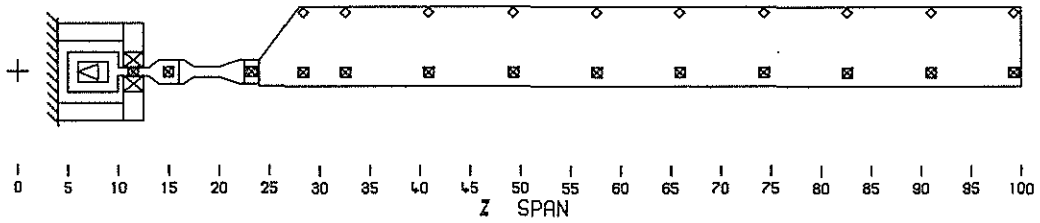

(c) accelerometer positions

× FLAP □ LAG ◇ TORSION

Fig 3 SPA instrumentation showing strain gauge and accelerometer positions for DLP rotor model

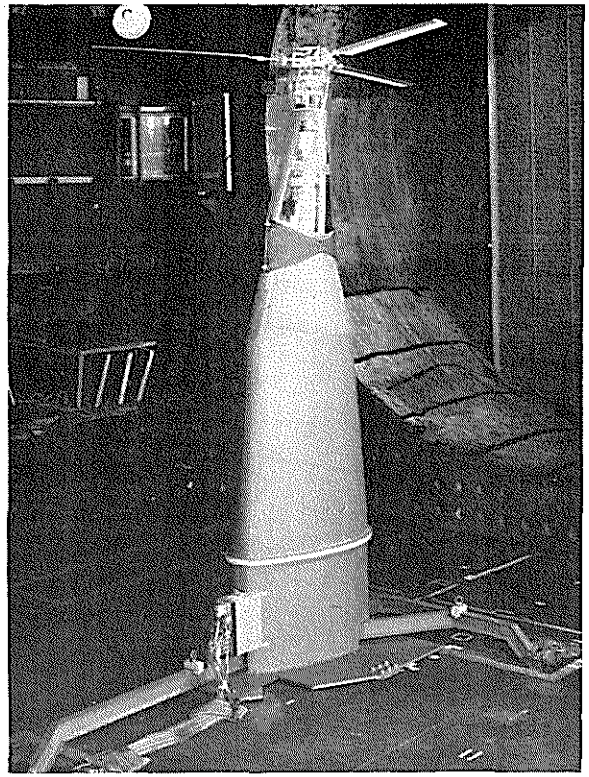

Fig 4 Rotor model in RAE 24ft wind tunnel

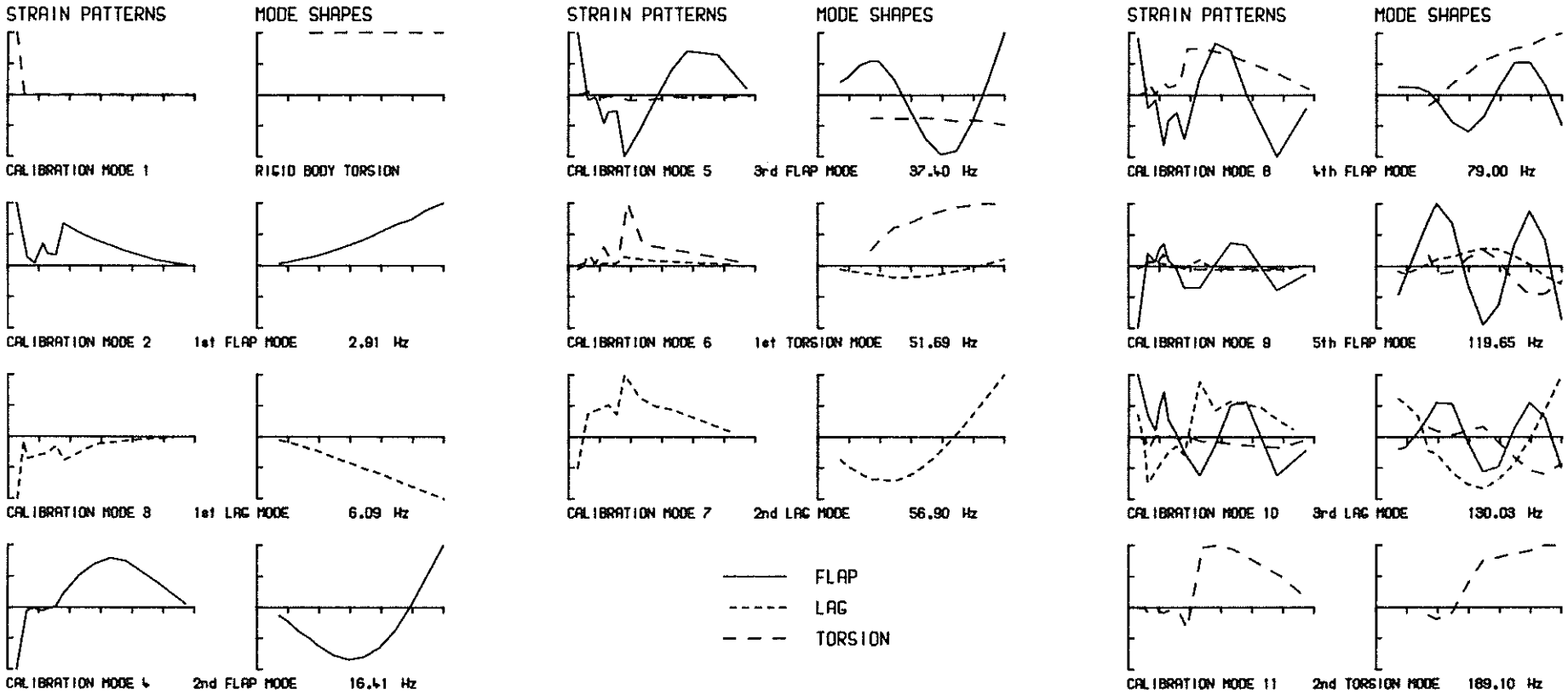

Fig 5 Non-rotating calibration modes used in SPA analysis of wind tunnel data for the DLP rotor model

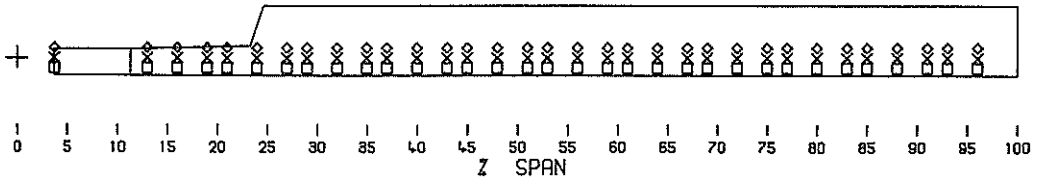

(a) strain gauge positions

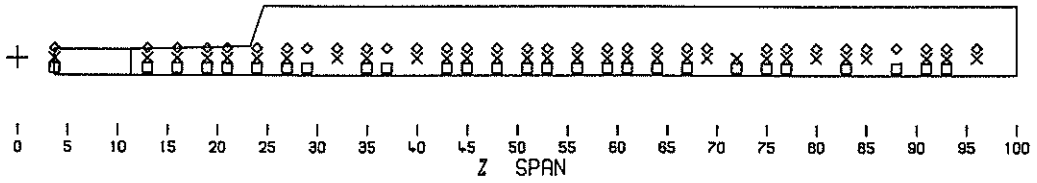

(b) strain gauge positions used in SPA

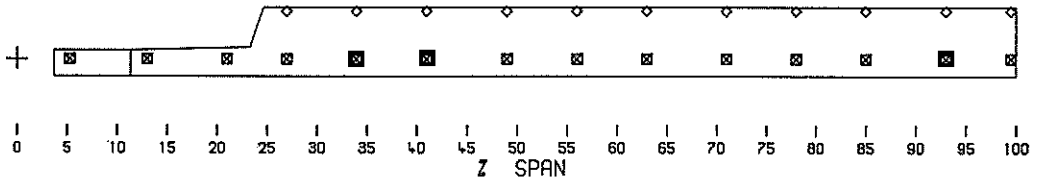

(c) accelerometer positions

× FLAP □ LAG ◇ TORSION

Fig 6 SPA instrumentation showing strain gauge and accelerometer positions for Puma helicopter main rotor system

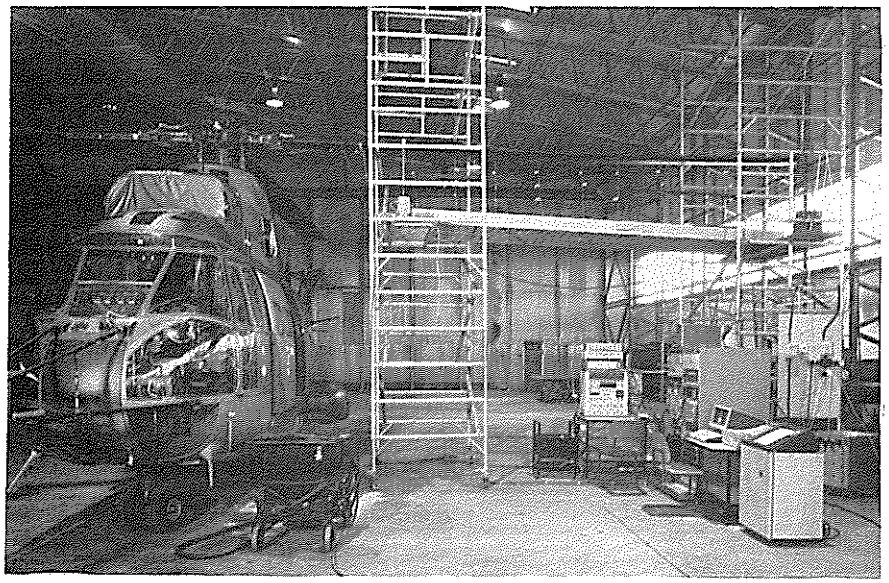

Fig 7 Puma helicopter XW241 during SPA ground calibration tests

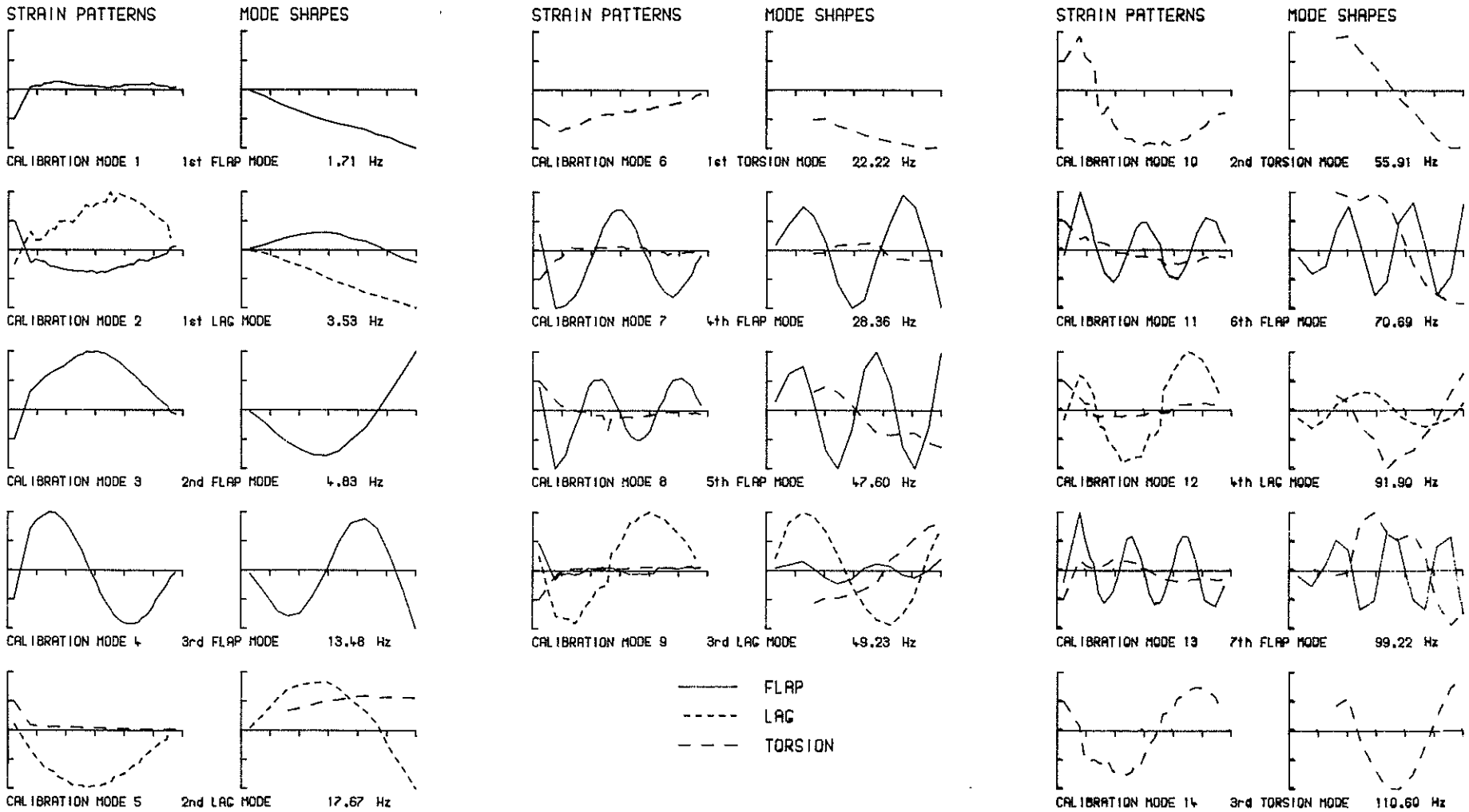

Fig 8 Non-rotating calibration modes used in SPA analysis of flight data for the Puma helicopter main rotor system

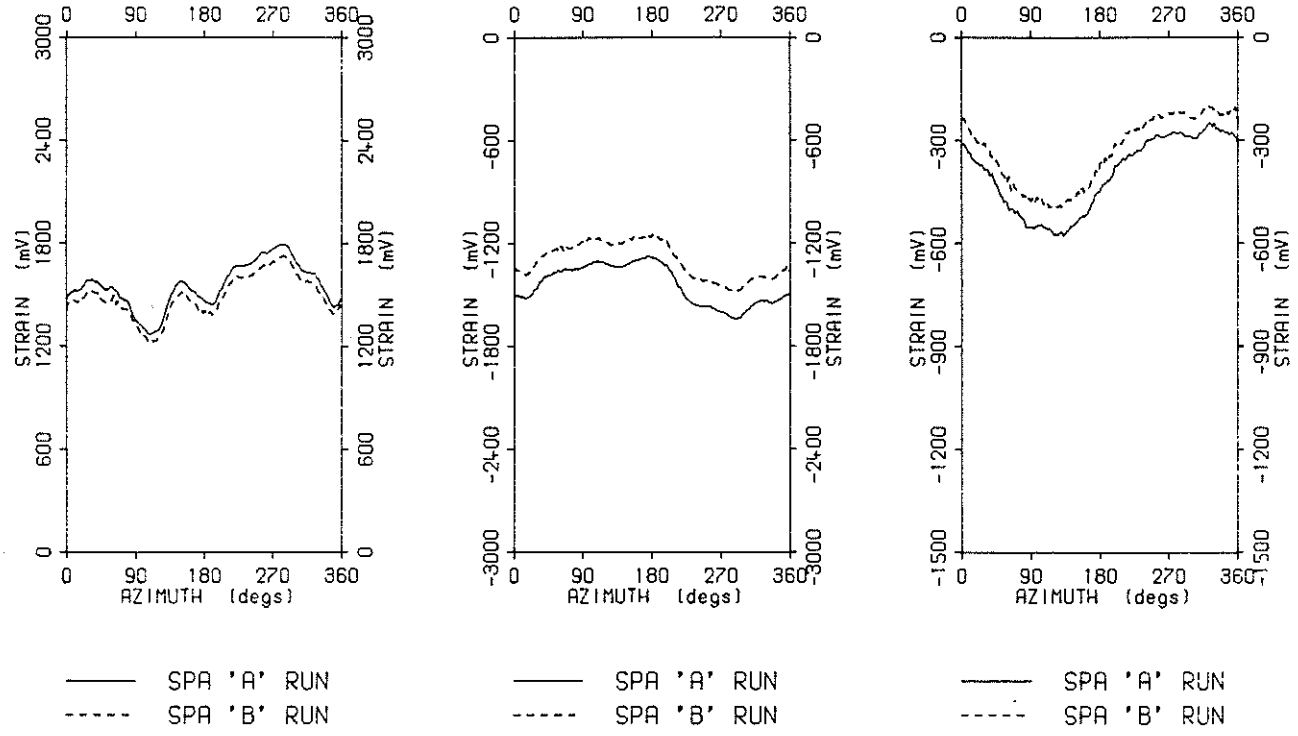

(a) blade flap strains at 30% rotor radius

(b) blade lag strains at 30% rotor radius

(c) blade torsion strains at 30% rotor radius

Fig 9 Comparison of wind tunnel SPA 'A' and 'B' runs
Rotor speed = 600 rpm Thrust = 900 N μ = 0.2

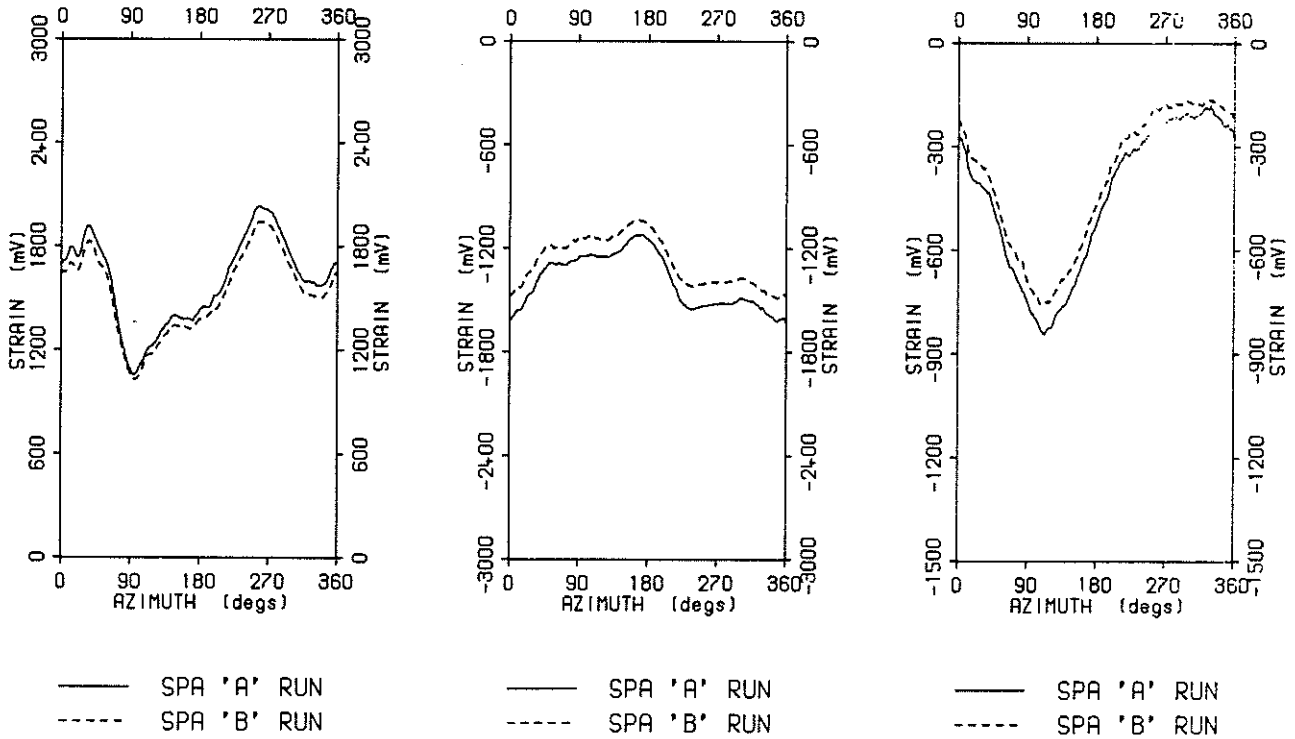

(a) blade flap strains at 30% rotor radius

(b) blade lag strains at 30% rotor radius

(c) blade torsion strains at 30% rotor radius

Fig 10 Comparison of wind tunnel SPA 'A' and 'B' runs
Rotor speed = 600 rpm Thrust = 900 N μ =0.34

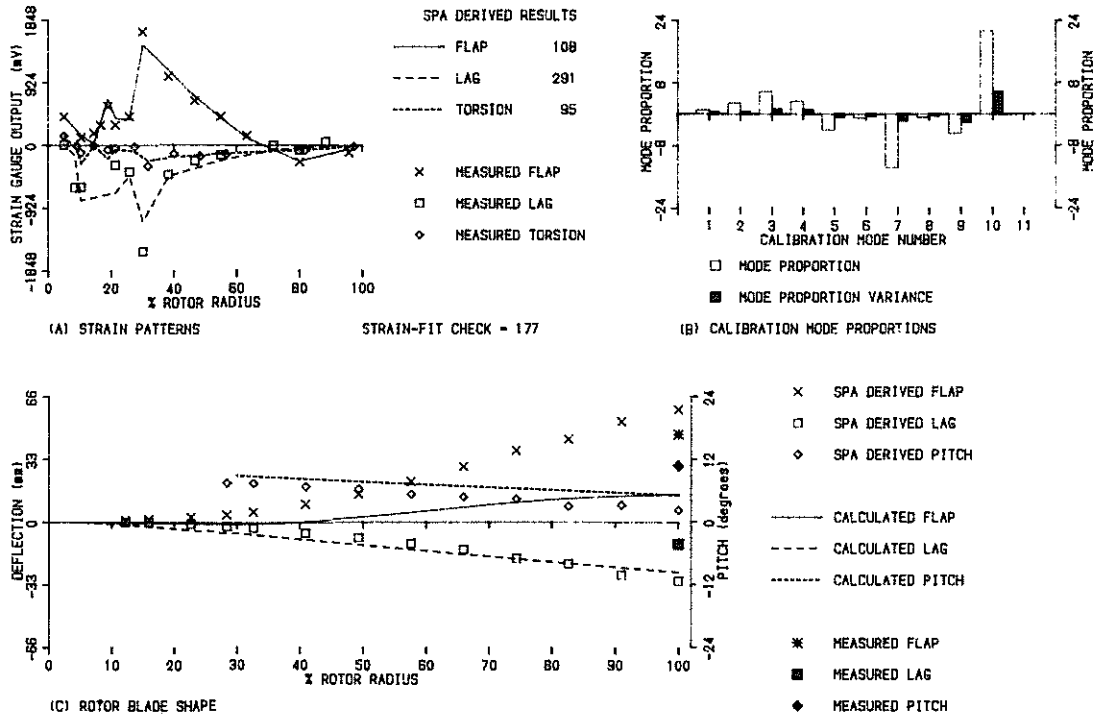

Fig 11 Example of results obtained for the DLP wind tunnel model
Rotor speed=600 rpm Azimuth=240^{o} Thrust=900 N μ=0.2

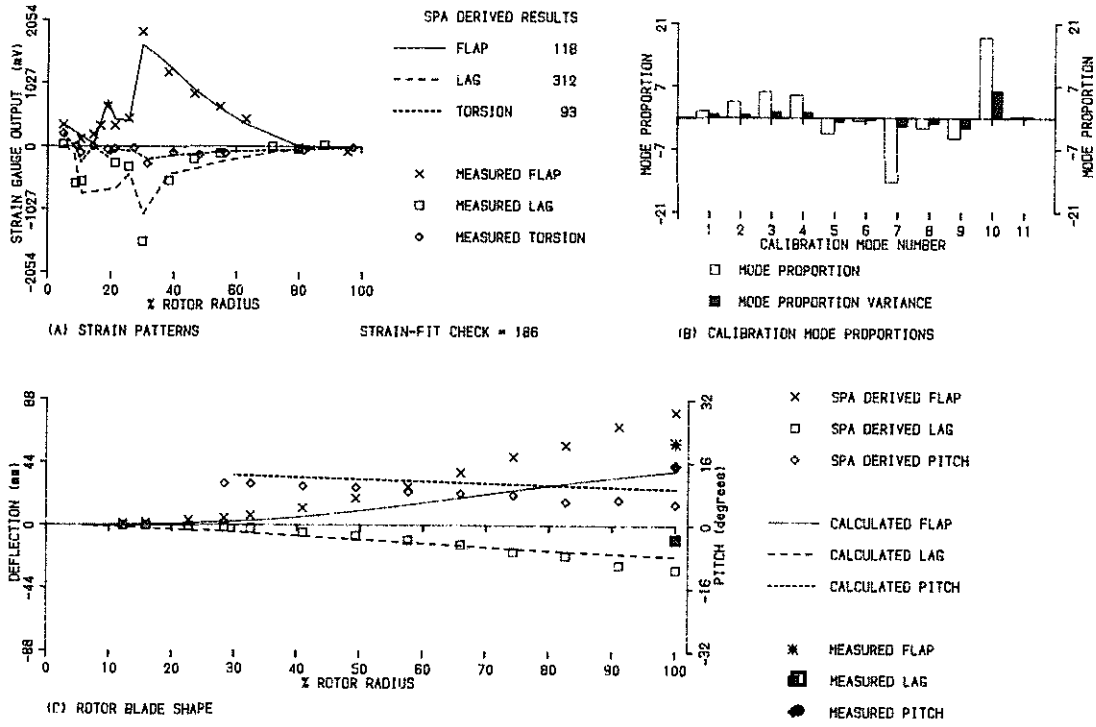

Fig 12 Example of results obtained for the DLP wind tunnel model
Rotor speed=600 rpm Azimuth=240^{o} Thrust=900 N μ=0.34

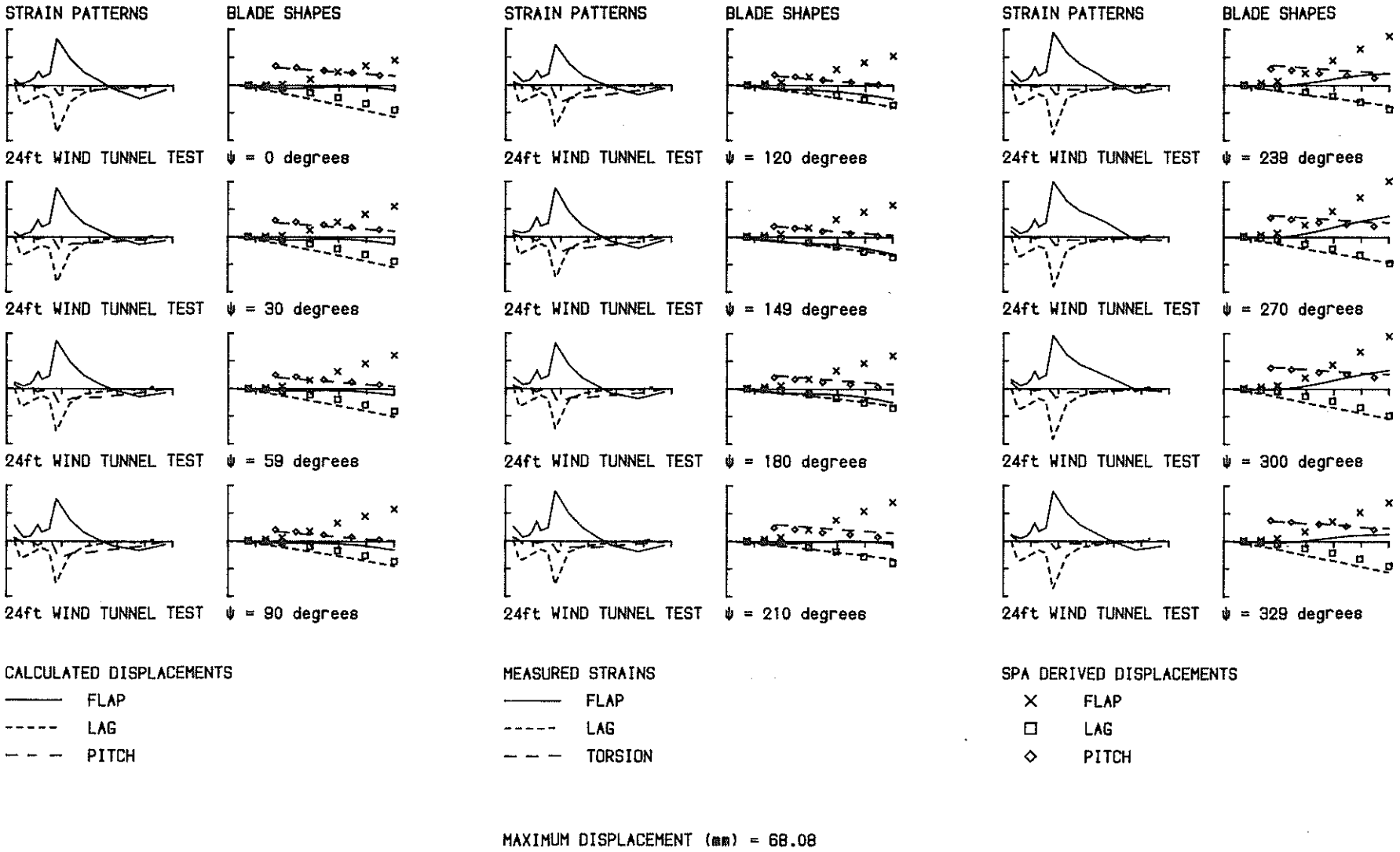

Fig 13 Wind tunnel model blade shape variation around the rotor disc
Rotor speed = 600 rpm Thrust = 900 N μ = 0.2

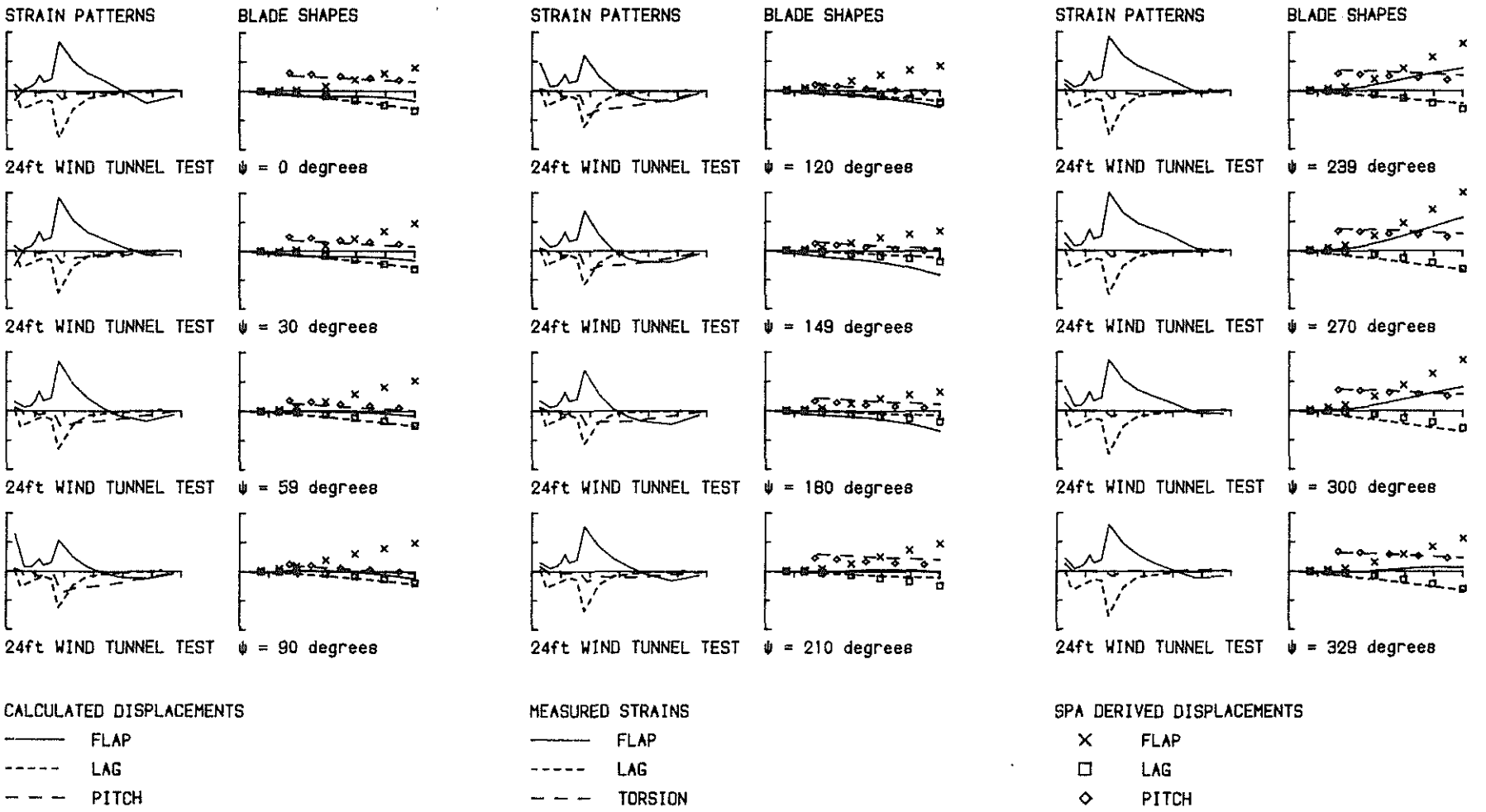

Fig 14 Wind tunnel model blade shape variation around the rotor disc
Rotor speed = 600 rpm Thrust = 900 N μ = 0.34

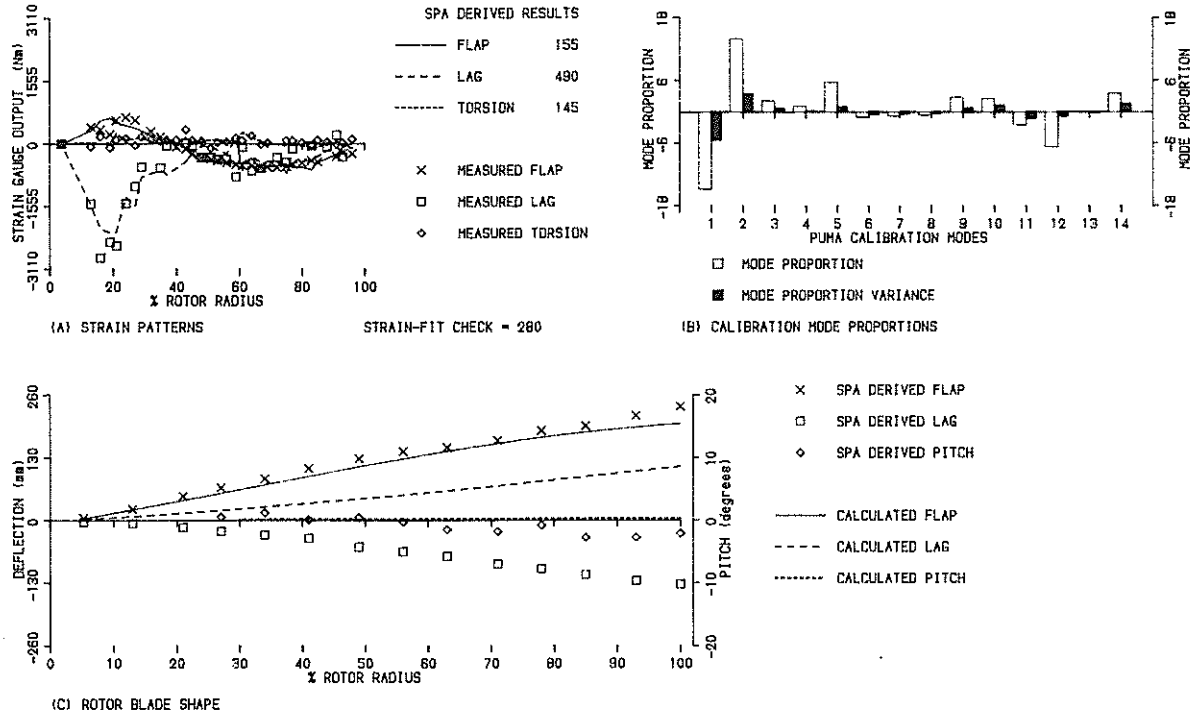

Fig 15 Example of elastic blade motion for the Puma rotor system
Speed = 80 kts Azimuth = 90° T_c = 0.09 μ = 0.193

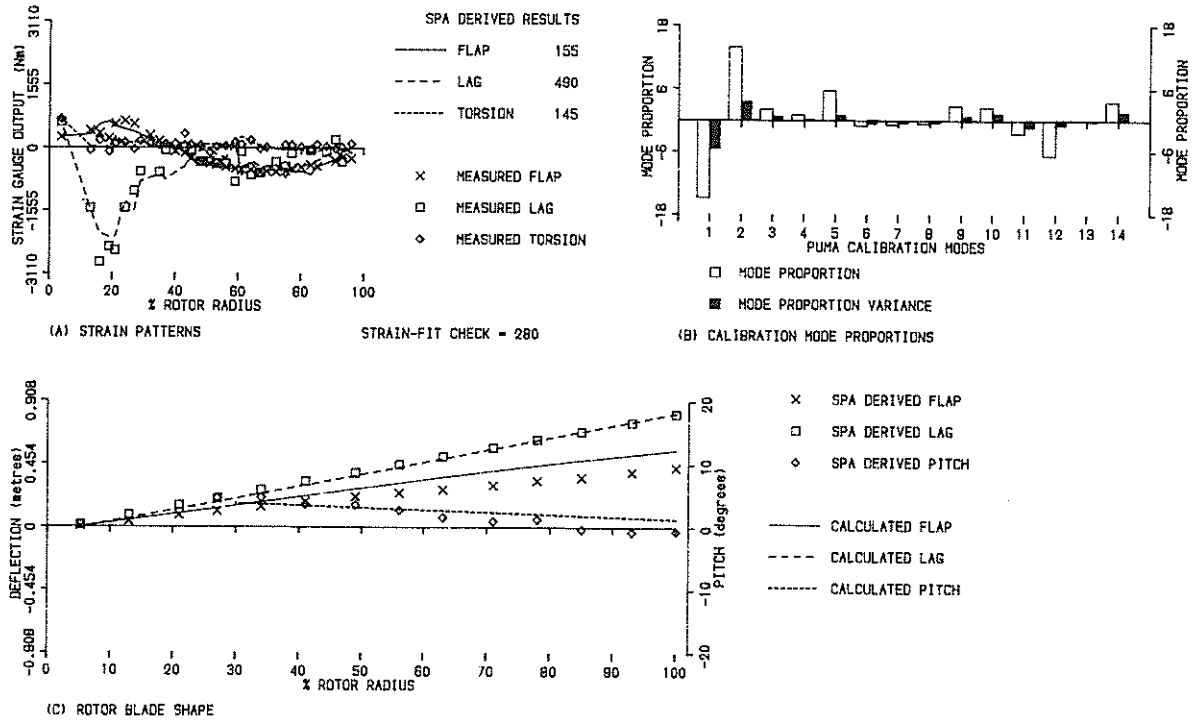

Fig 16 Example of total blade motion for the Puma rotor system
Speed = 80 kts Azimuth = 90° T_c = 0.09 μ = 0.193

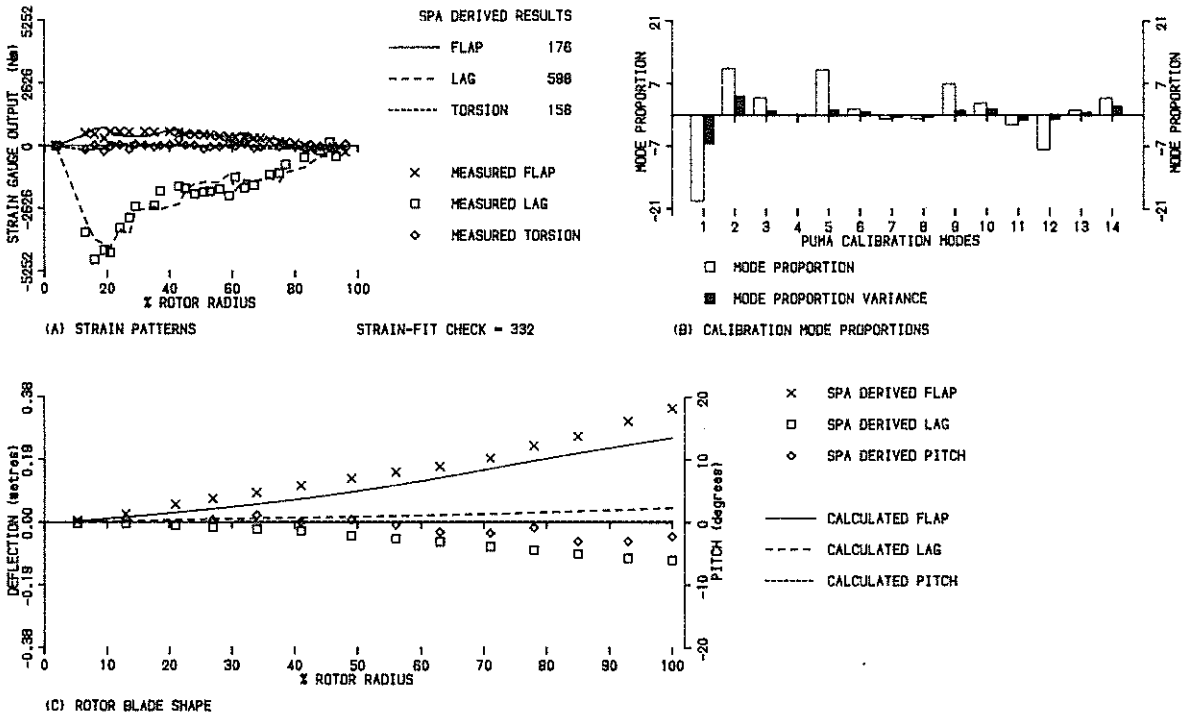

Fig 17 Example of elastic blade motion for the Puma rotor system
Speed = 80 kts Azimuth = 270^{o} $T_c = 0.09$ $\mu = 0.193$

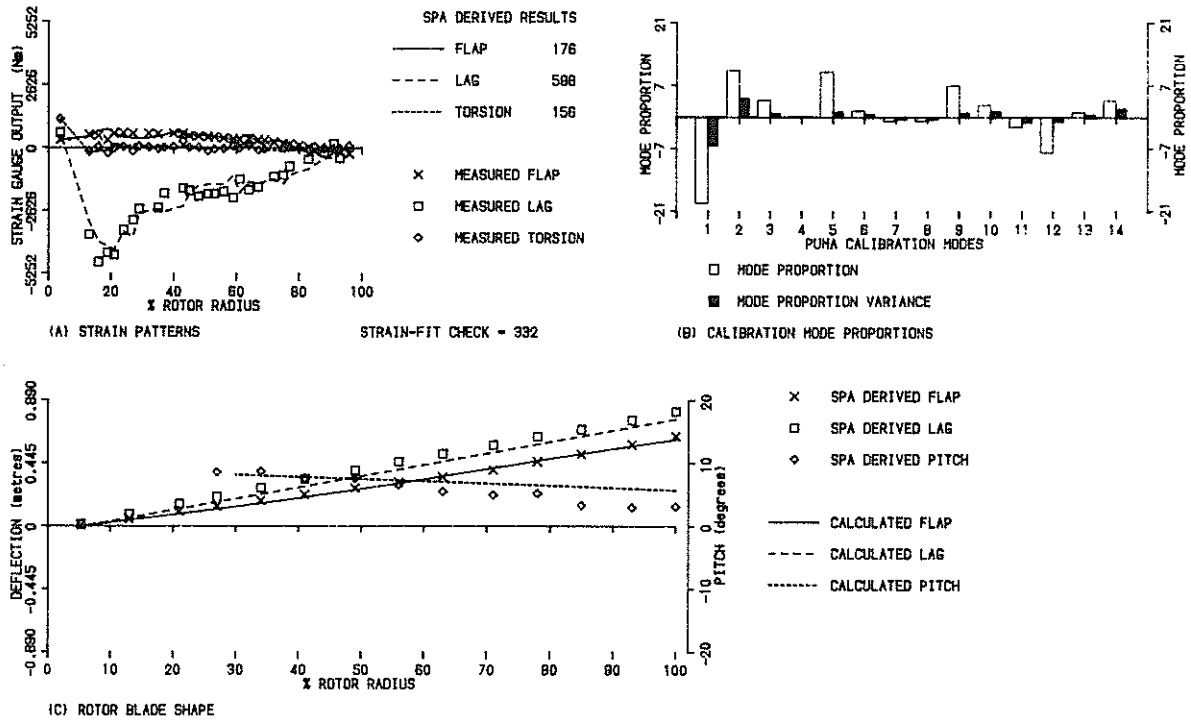

Fig 18 Example of total blade motion for the Puma rotor system
Speed = 80 kts Azimuth = 270^{o} $T_c = 0.09$ $\mu = 0.193$

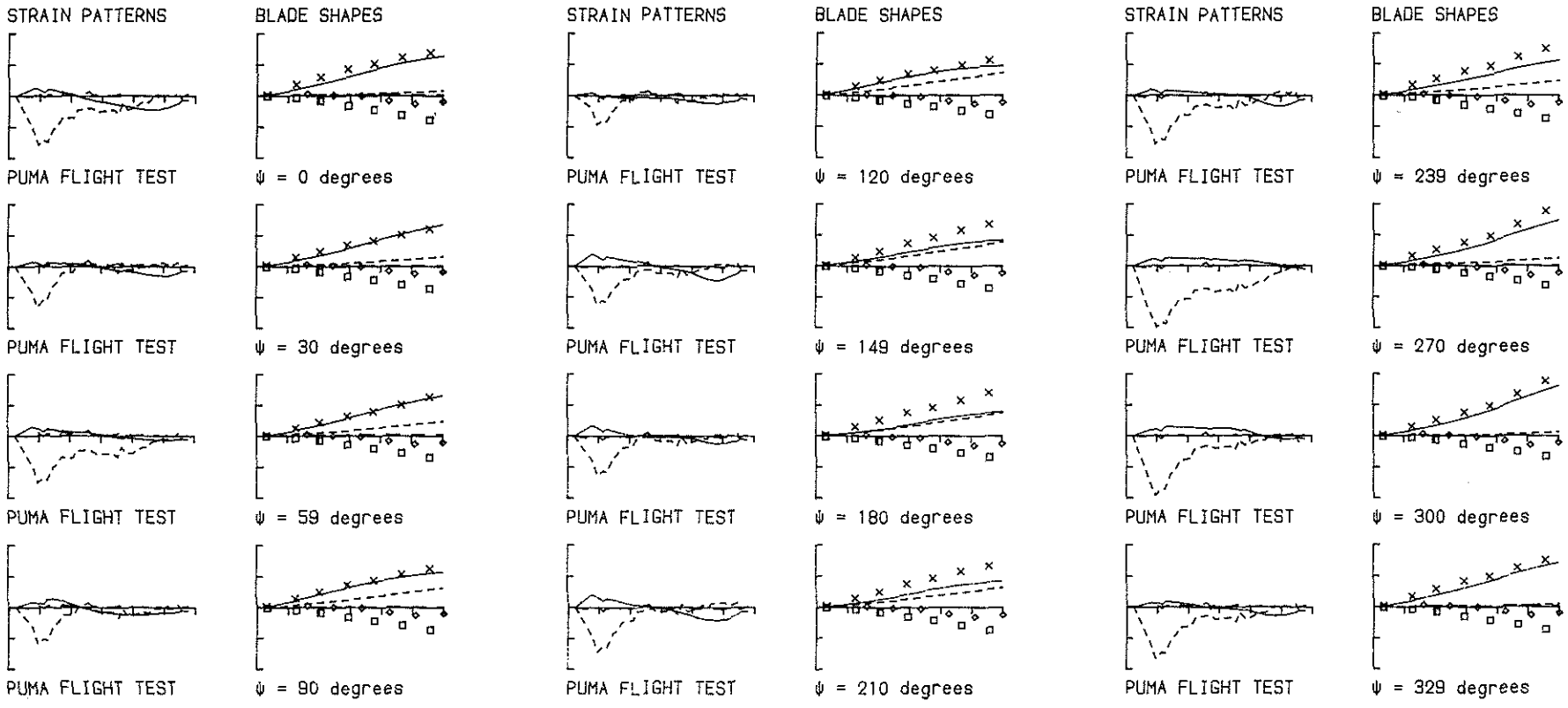

Fig 19 Puma rotor elastic blade shape variation around the rotor disc
Speed = 80 kts Thrust = 6065 kg T_c = 0.09 μ = 0.193

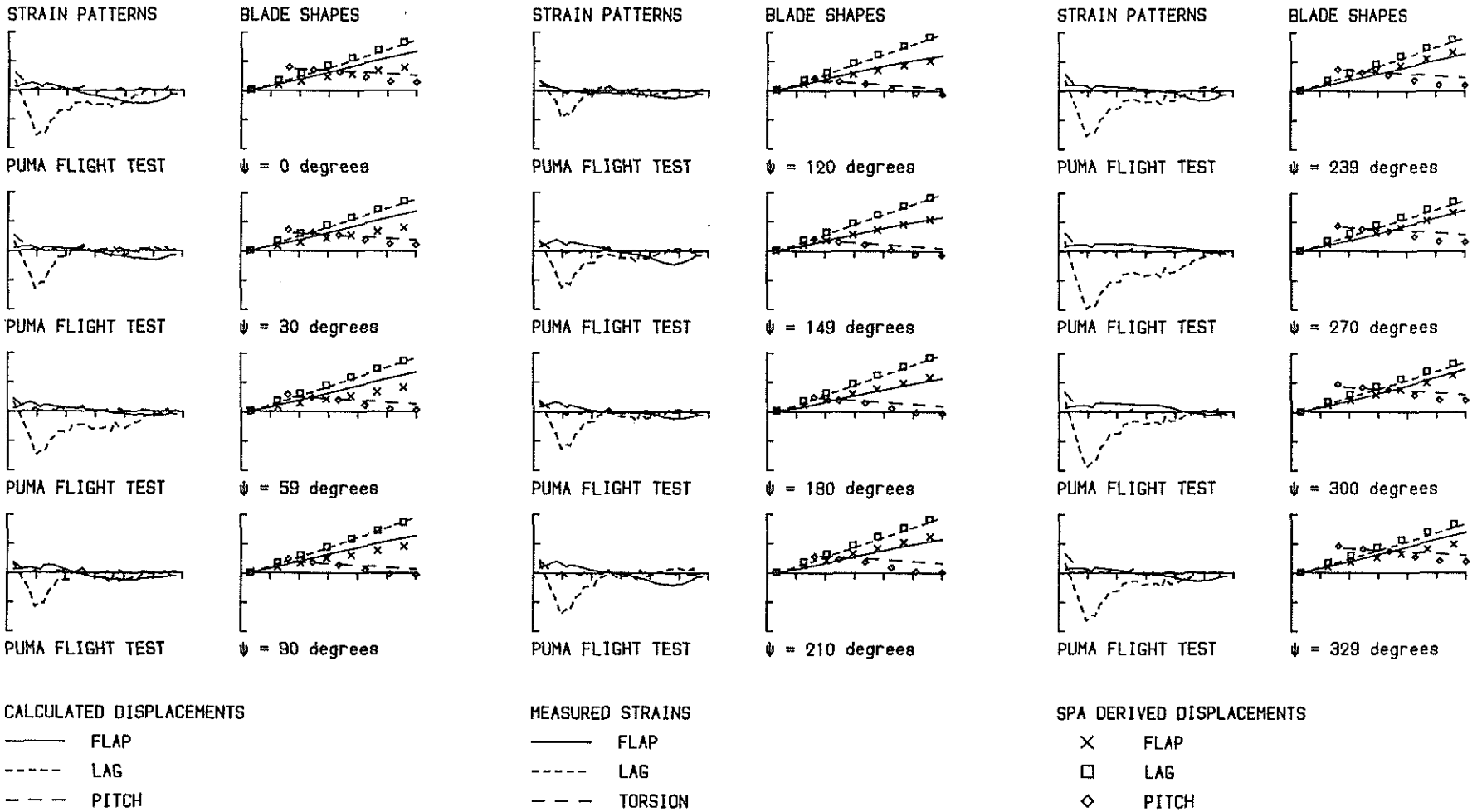

Fig 20 Puma rotor total blade shape variation around the rotor disc
Speed = 80 kts Thrust = 6065 kg T_c = 0.09 μ = 0.193